ACS APPLIED MATERIALS & INTERFACES

www.acsami.org

Research Article

Photoinduced Charge Transfer and Trapping on Single Gold Metal Nanoparticles on TiO_2

Monica Luna,* Mariam Barawi, Sacha Gómez-Moñivas, Jaime Colchero, Micaela Rodríguez-Peña, Shanshan Yang, Xiao Zhao, Yi-Hsien Lu, Ravi Chintala, Patricia Reñones, Virginia Altoe, Lidia Martínez, Yves Huttel, Seiji Kawasaki, Alexander Weber-Bargioni, Victor A. de la Peña ÓShea, Peidong Yang, Paul D. Ashby,* and Miquel Salmeron*

Cite This: *ACS Appl. Mater. Interfaces* 2021, 13, 50531−50538

Read Online

ACCESS | Metrics & More | Article Recommendations | Supporting Information

ABSTRACT: We present a study of the effect of gold nanoparticles (Au NPs) on TiO_2 on charge generation and trapping during illumination with photons of energy larger than the substrate band gap. We used a novel characterization technique, photoassisted Kelvin probe force microscopy, to study the process at the single Au NP level. We found that the photoinduced electron transfer from TiO_2 to the Au NP increases logarithmically with light intensity due to the combined contribution of electron−hole pair generation in the space charge region in the TiO_2−air interface and in the metal−semiconductor junction. Our measurements on single particles provide direct evidence for electron trapping that hinders electron−hole recombination, a key factor in the enhancement of photo(electro)catalytic activity.

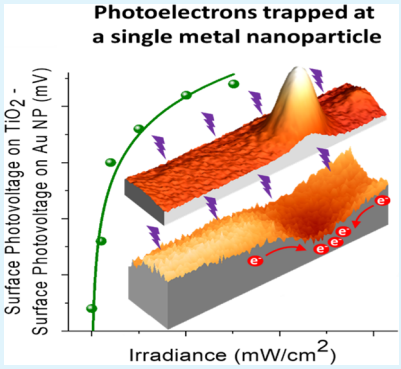

KEYWORDS: *charge transfer, photovoltage, Kelvin probe force microscopy, atomic force microscopy, TiO_2, metal nanoparticles, photoelectrocatalysis*

INTRODUCTION

Many technologies of societal importance, such as CO_2 conversion to fuels, hydrogen production by water splitting, and new materials with self-cleaning and antifogging properties, are based on heterogeneous photocatalysis.[1−3] A limitation of these technologies is their low efficiency due to the high recombination rate of the photogenerated electron−hole pairs. Strategies to increase charge separation in the photocatalyst include decorating the surface with metal nanoparticles. The Schottky barrier at the metal−semiconductor interface and the associated electric field in the space charge region increases the efficiency of separation of electrons and holes and their diffusion.[4] Under UV illumination, metal NPs in direct contact with the semiconductor can efficiently attract photogenerated electrons from the TiO_2 conduction band, while holes are accumulated in the valence band of the oxide. This spatial separation of charge carriers results in an increased lifetime and, therefore, the catalytic efficiency. This strategy significantly increases the photocatalytic reduction efficiency of CO_2, the selectivity toward methane synthesis,[5,6] the photoproduction of hydrogen,[7] and the photo-oxidative degradation of NO by increasing the efficiency by 700% relative to unmodified TiO_2.[8] In addition, studies reveal that interfacial sites at the TiO_2−Au NPs activate adsorbed molecular species.[9,10] However, the charge-transfer process at the TiO_2−metal NP junction scale is poorly understood, and yet, it is key to enable the design of more efficient photoactive materials.

Another recent strategy to improve the catalytic performance is the use of plasmonic properties of Au nanoparticles. The enhancement of the local electric field on the metal nanoparticle increases the local transition probability of an instantaneous one-photon reaction, favoring the photochemical reactions on and near the surface of the metal.[11] The enhanced near-field in metal NPs has been shown to boost the excitation of electron−hole pairs in TiO_2 and therefore increase the efficiency of the photocatalysis.[12] Nonetheless, it should be taken into account that the presence of metal nanoparticles could also result in an enhancement or quenching, depending on the distance between the metal and the TiO_2.[13]

The Au/TiO_2 interface has been the subject of theoretical and experimental investigation. Theoretically, metal−semi-

Received: July 19, 2021
Accepted: October 1, 2021
Published: October 13, 2021

conductor contact theory[14] and density functional theory[15] are most frequently employed. On the experimental side, ultrahigh vacuum studies using scanning tunneling microscopy and atomic force microscopy (AFM) have been used for atomic-scale characterization of TiO_2 sensitized with metal clusters[16,17] and with organic dyes used in solar cells,[18] which contributed to our current knowledge of charge transfer in model metal/TiO_2(110) systems,[19] including Pt[20] and small Pt clusters.[21] The effect of light exposure has been studied using photoluminescence,[22] photoelectron spectroscopy, and surface photovoltage (SPV) techniques[4] and used for the evaluation of photocatalytic activity.[23] These experiments suggest that electrons are transferred from TiO_2(110) to the Pt clusters.[20] When the sample was afterward exposed to air and to N_2 environments, no net charge transfer was detected,[24] obviating the need for controlled experiments under ambient conditions. In addition, all these studies were performed over large areas, which average the effect of large numbers of NPs of different shapes and sizes and thus do not provide the critical microscopic insights needed to understand charge transfer between single NPs and the substrate.

Here, we focus on single Au NPs using Kelvin probe force microscopy (KPFM), which provides nanometer-scale resolution topographic and contact potential difference (CPD) maps. In addition, to overcome the averaging effect mentioned above, we focused a UV photon beam ($h\nu$ > 3 eV) onto the AFM tip while imaging. This operation mode, photoassisted Kelvin probe force microscopy (PA-KPFM), allowed us to map out the spatial topography and SPV structure on and around single Au NPs on TiO_2 under illumination and their charge transfer and trapping properties in different environments. Our PA-KPFM results provide information on charge generation and transfer at the interface of individual Au NPs on TiO_2. We then compared our results with those from space-averaging electrochemical techniques to reveal the fundamental processes that determine the enhancement in photocatalytic H_2 production.

RESULTS AND DISCUSSION

Photoexcited Carrier Generation on TiO_2 in Gas-Phase Environments. We studied the bare TiO_2(110) surface during illumination with supra-bandgap energy light (365 nm wavelength, corresponding to 3.4 eV) by scanning an AFM $PtIr_5$ tip in noncontact mode while simultaneously acquiring topographic (Figure 1a) and CPD (V_{CPD}) images (Figure 1b). During the first minute (top 25 lines of the image), the illumination was off, and then it was turned on for the remainder of the image. After turning the light on, a sudden increase of the V_{CPD} was observed by the change in contrast after line 25. The total light exposure time from line 25 to line 305 at the bottom of the image was 16 min. Figure 1c shows a V_{CPD} profile extracted from Figure 1b after subtracting the profile obtained in the dark. The resulting difference corresponds to the SPV.[25] In the dark, the V_{CPD} was around +532 mV, with the positive value reflecting the higher work function of the metallic $PtIr_5$ tip relative to the oxide substrate, as illustrated in the Supporting Information (Figure S1).

After the initial rapid increase, the SPV continued to increase slowly (light-purple region in Figure 1c) and saturated after about 5 min. The increase in SPV is due to the accumulation of positive carriers (holes) on the surface of TiO_2 as expected from its n-type nature, which produces an

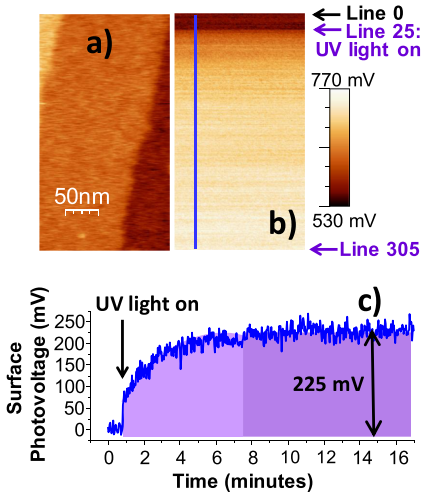

Figure 1. (a) PA-KPFM topography (the color scale span: 1.83 nm) and (b) V_{CPD} images of bare TiO_2(110) acquired simultaneously. During the first minute, there was no UV illumination (lines 0 to 25). In the following lines, the UV illumination intensity was 0.40 mW/cm^2. (c) Surface photovoltage (SPV = $V_{CPD\text{-light}} - V_{CPD\text{-dark}}$) vs time (profile along the blue line in b). A total increase of 225 mV is measured.

electric field in the surface space charge region that drives the photogenerated holes to the surface. Although e−h pairs are generated throughout the penetration depth of the photons, which is on the order of micrometers, most of them recombine and only a fraction of those generated within the depletion region reach the surface. These charge carriers can be temporarily captured on traps created by defects. The photoexcited holes accumulated at the surface counter-balance the built-in surface potential, causing the bands to flatten partially. The flattening or downward bending of the TiO_2 bands upon illumination manifests in a decrease in the sample work function so that the V_{CPD} is more positive (larger) under illumination, as shown in the Supporting Information (Figure S2). Electron excitation from defect states can also occur under UV-light illumination.[26]

When the light was turned off, the time to recover the original SPV value was on the order of days due to the long lifetime of trapped holes on the surface of the TiO_2 in the inert N_2 atmosphere of our chamber. However, in the presence of hole-scavenger species, the recovery time decreased to a few minutes. We demonstrated this by introducing methanol, an active reducing agent, into the KPFM chamber with the N_2 (Figure S3).

Photoexcited Carriers on TiO_2 in Electrolyte Environments. In parallel experiments, photovoltage (PV) measurements were carried out in a photoelectrocatalytic cell filled with a 0.5 M Na_2SO_3 aqueous solution at pH 9. The experiments were carried out both with bare TiO_2 and with ligand-free Au NPs covering the TiO_2(110). Electron exchange across the TiO_2−electrolyte junction equilibrates the sample Fermi level with the redox potential of the SO_3^{2-}/SO_4^{2-} pair, which is located in the band gap of TiO_2. As a result, the bands of the oxide shift upward at the interface, as illustrated in Figure 2a. When the light was turned on, a fast negative change in the sample voltage versus Ag/AgCl, followed by a slower decrease reaching a quasi-steady state, was observed. The photogenerated carriers (holes) move to the surface of the semiconductor, where they are compensated by negatively

https://doi.org/10.1021/acsami.1c13662
ACS Appl. Mater. Interfaces 2021, 13, 50531−50538

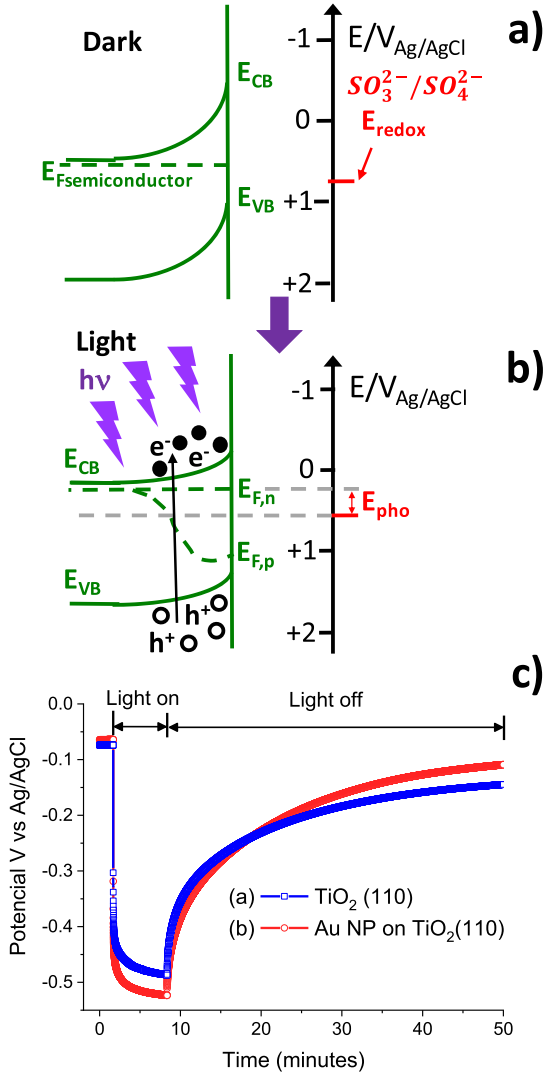

Figure 2. PV in an electrochemical cell containing 0.5 M Na_2SO_3 aqueous solution at pH 9. (a) When the TiO_2 sample is submerged in the electrolyte, the Fermi level is pinned at the redox potential level of the electrolyte (in this case, SO_3^{2-} E_{redox}), which is located in the TiO_2 band gap. The bands shift to more positive potentials for an n-type semiconductor, with a resultant upward bending. (b) Under UV light, photogenerated minority carriers (holes) move to the surface where they are compensated by negatively charged species from the electrolyte, decreasing the band bending and causing the potential to move to more negative values (vs Ag/AgCl reference electrode). (c) Sample potential measured under illumination by band gap UV light on TiO_2 with and without Au NP as a function of time.

charged species from the electrolyte, leading to a decrease in the band bending. This is in line with the SPV measurements by PA-KPFM in the gas environment described earlier, where positive values indicate the presence of more holes at the surface.

A noticeable difference in recovery time to the original PV value after turning off the illumination is observed between the PA-KPFM experiments performed under a gas atmosphere (Figure 1) and the photoelectrochemistry results (Figure 2). In the electrolyte, the decay time is approximately a couple of hours, while in a N_2 atmosphere, it takes several days. The difference is due to the presence of SO_3^{2-} charge-scavenging ions in the solution, which react with the created holes and transfer the charge to the solution, similar to the effect of methanol in the gas-phase experiments described above.

Effect of Au NPs on Photoexcited Carriers in TiO_2 in Gas-Phase Environments. After studying the charge generation and photovoltaic behavior of bare TiO_2, we focused on the effect of the Au NPs on the photovoltaic and chemical properties of TiO_2. Figure 3 shows noncontact amplitude-

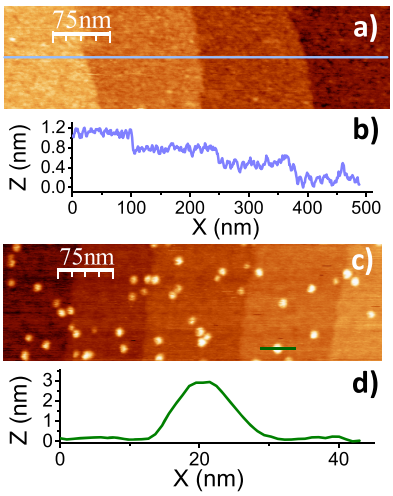

Figure 3. AFM topographic images of TiO_2(110). (a) Without and (c) with deposited gold nanoparticles. (b,d) Height profiles along the lines in (a,c), respectively.

modulation topographic images of TiO_2(110) before (Figure 3a,b) and after decoration with ligand-free Au NPs (Figure 3c,d). The surface coverage is 0.42%. The height profiles along the lines in the figure indicate a step height of 0.33 nm on the TiO_2 surface, and a Au NP height of 3.0 ± 0.6 nm, which corresponds to the NP diameter. A histogram of the Au NP size for this sample is shown in Figure S4 in the Supporting Information.

Using PA-KPFM, we then measured the CPD and the effect of light intensity around individual Au NPs in the dark and under UV illumination. As shown in Figure 4a, in the dark, the CPD is 12 mV lower (more negative) on top of the 3 nm Au NP than the surrounding TiO_2. The width of the CPD profiles is about 50 nm, which is about the diameter of the tip (see tip apex TEM image in Figure S5). The difference in CPD measured on top of the Au NP compared to the TiO_2 substrate reflects the higher work function of Au (W_{Au} = 5.1 eV) compared to that of TiO_2(110) (W_{TiO2} = 4.2 eV) that leads to a transfer of negative charge from TiO_2 to the Au NP, which creates a Schottky barrier at the Au/TiO_2 interface with a calculated depletion length[14] of about 12 nm for NPs of 3 nm diameter. Details of this calculation can be found in the Supporting Information (Figure S6). Although the small size of the Au NP is known to lead to a smaller work function than that of bulk Au,[27] the small measured value of 12 mV compared to the difference in the work functions of bulk Au and TiO_2 (Figure 5) is mostly due to averaging effects due to the large tip apex radius. A theoretical modeling (Supporting Information sections 7 and 8) shows that a significant reduction in the measured surface potential difference between TiO_2 and the Au NP (Figure 5b) of 87% is indeed expected with respect to bulk Au due to averaging (Figure 5). The model also indicates that the field produced by the charge in

https://doi.org/10.1021/acsami.1c13662
ACS Appl. Mater. Interfaces 2021, 13, 50531−50538

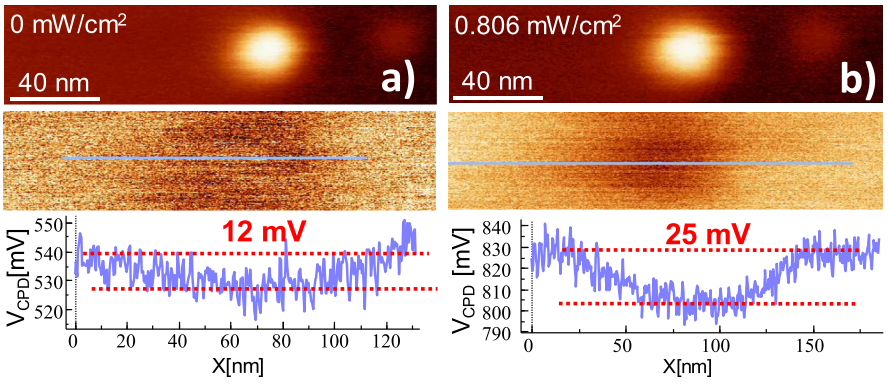

Figure 4. Topography (top) and V_{CPD} (bottom) images of a 3 nm diameter Au NP on bare TiO_2(110) (a) in the dark and (b) under UV illumination. V_{CPD} profiles are shown at the bottom. Color scale in topography: (a) 3.6 nm and (b) 4 nm. A CPD image of a larger sample area can be found in the Supporting Information (Figure S10).

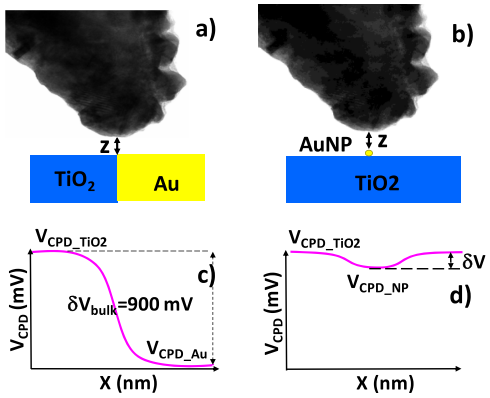

Figure 5. Calculated averaging effects of the CPD measured by the tip on Au NP versus bulk Au (details in the Supporting Information, sections 7 and 8). (a) Scheme where KPFM is performed on a sample consisting of bulk TiO_2 and Au; (b) same for a Au NP on the TiO_2 surface. The theoretical modeling predicts a significant reduction on the CPD (δV) in (b) due to the small size of the Au NP with respect to the tip.

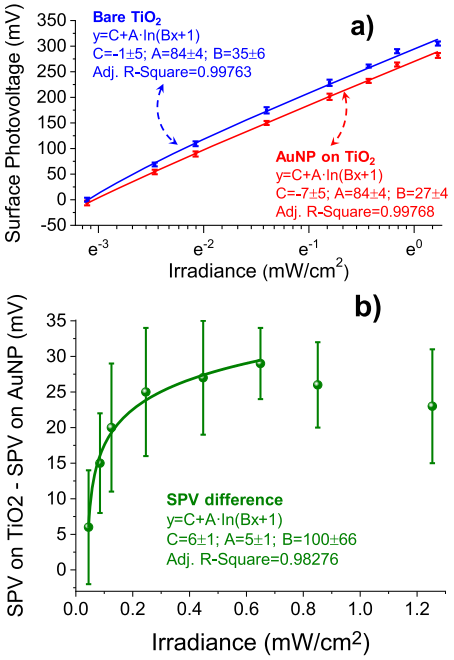

Figure 6. (a) Surface PV vs irradiance with 365 nm wavelength light, with fits to the logarithmic functions for bare TiO_2 (blue) and for the Au NP on the TiO_2 (red). (b) Difference between SPV on bare TiO_2 and SPV on the Au NP as a function of irradiance. The data in (a) is plotted with a logarithmic X-axis, while the data in (b) has a linear axis. The differences shown in (b) underestimate the real difference because the SPV on top of the Au NP averages with the value of the SPV on the surrounding area, as explained in Figure S6 of the Supporting Information.

the NP is reduced by that emanating from the image charge of opposite sign in the supporting TiO_2.

Under illumination, the CPD on top of the Au NP is lower by 25 mV relative to the surrounding TiO_2, larger than the value in the dark by factor 2. To understand this result, we should consider that there are two space charge regions in the TiO_2, one in the vicinity of the Au NP/TiO_2 (metal–semiconductor space charge region) and the other at the interface between the TiO_2 surface and the gas away from the NP (Supporting Information, Figure S6a). Therefore, with UV irradiation, the photogenerated carriers will diffuse to the two interfaces in different amounts. Our results indicate that the Au NPs are more negative during illumination than the surface areas of TiO_2 farther away from them. The resulting differential charging was measured by plotting the difference in V_{CPD} of Au versus that of TiO_2 as a function of irradiance (Figure 6a), with each point representing the mean value of 144 data points. Figure S11 (Supporting Information) shows simultaneous topography and CPD images at each value of the irradiance. As the light power increases, the SPV increases, reaching a value of 300 mV at an irradiance of 1.25 mW/cm^2. The logarithmic dependence on light intensity is typical for charge separation at the built-in potential (before saturation) in the space charge region,[28] which decreases the band bending due to accumulation of positive carriers at the surface. In the fit, $\mathrm{SPV} = \eta\frac{k_B T}{q}\log_e(BI + 1)$, η and B are proportionality constants that depend on the state of the surface and on the photoelectromotive force (emf) mechanism, and I is the illumination intensity. From the fit to the data, we obtain $\eta \approx 3$ $\left(\frac{k_B T}{q}\right)$ = 25.7 mV at T = 300 K. Values above 2 are characteristic of significant trapping.[28,29] In Figure 6b, we plot the SPV difference between the values on top of Au and on the bare TiO_2, which can be fitted by a logarithmic function with a coefficient of 6 ± 1, indicating that the Au NPs are efficient at trapping negative charge as the irradiance increases. The Au

https://doi.org/10.1021/acsami.1c13662
ACS Appl. Mater. Interfaces 2021, 13, 50531−50538

NPs are more efficient than suggested by the measurement because the SPV measured on top of the Au NPs is an average between that on the Au and that of the surrounding area within a radius of the order of the tip diameter. Although the maximum difference measured depends on parameters such as tip size, the logarithmic trend (Figure 6a,b) was found in all the experiments. Figure 6b also shows that after increasing from 0 to 0.6 mW/cm^2, the SPV diminishes at high intensities. This can be attributed to the Dember effect,[30] where high irradiance gives rise to differences in photogeneration rates along the photon penetration depth and space charge region. This, coupled with the different electron and hole diffusivities decreases the value of the SPV due to the higher hole concentration near the TiO_2 surface.[1,31]

Effects on the SPV from defects and impurities of the TiO_2 surface are not expected to play a significant role here. For example, surface states from O-vacancies should not be present in appreciable amounts due to the annealing treatment performed under a flux of clean air. Finally, the presence of organic contamination, such as small-chain carboxylic acids, is not expected to affect photocharge separation because the organic compounds do not absorb UV light efficiently. Moreover, organic compounds will be removed from the surface under UV illumination, which oxidizes and eliminates them from the surface. To demonstrate the photo-degradation of carbonaceous species, we performed experiments using highly surface-sensitive sum frequency generation spectroscopy (Supporting Information, section 11).

It is interesting to note that gold NPs absorb light from the visible region of the spectra (530 nm), attributed to plasmon resonance wavelength. However, in Au NPs on TiO_2 systems,[5] the UV irradiation does not show a significant effect in the SPR of Au NPs. This is mainly because the main portion of the UV irradiation is absorbed by TiO_2. The fraction that can be absorbed by the Au NPs generates hot electrons[32] that quickly recombine, leading to a negligible effect in the charge dynamic processes. In some cases, this recombination could lead to a local increase of the temperature in the Au NPs (hot spot), which could have some effect in the catalytic reaction.

Effect of Au NPs on Photoexcited Carriers on TiO_2 in Electrolyte Environments. As shown in Figure 2, in an electrochemical environment, the samples with Au NPs also show a photovoltage difference (vs Ag/AgCl reference) relative to bare TiO_2, although in this case, the value represents an average over the whole surface. In the electrochemical environment, a large change in photovoltage is also observed when Au NPs are present, also following a logarithmic behavior versus irradiance (Supporting Information, Figure S15c). The PV on the sample with Au NPs reaches a larger minimum, implying that more trapped charges are available on this surface than on the surface without Au NPs. Moreover, electrochemical impedance spectroscopy (EIS) confirms that the presence of Au NPs improves the conductivity of electrons through the TiO_2 to the solution and determines the flat band potential (V_{FB}) and Fermi level position of both samples (Supporting Information, Figures S16 and S17). These results demonstrate the presence of a change in band positions when Au NPs are supported in the surface (Figure S18b). Photoelectrocatalytic experiments (in aqueous solution) were performed to evaluate the benefits of Au NPs on catalyst performance. Under UV illumination, we found that the accumulated hydrogen production increases during illumination and reaches a value of 1950 μmol H_2 at the end of the reaction (Figure 7), which is more than 30% higher than in bare TiO_2. Photocurrent measurements exhibited a similar

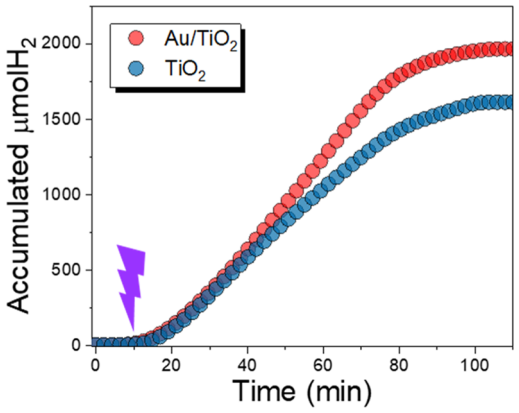

Figure 7. Accumulated H_2 production for TiO_2 and Au NPs on TiO_2 under UV irradiation at 0.7 V (vs Ag/AgCl) during 1 h. The light was turned on after a stabilization period of 10 min.

behavior, showing a current decrease, in the case of TiO_2, more accentuated even at the first stage of the reaction (Figure S19). This behavior indicates that in both cases, the main active sites for photoelectrocatalytic reactions are located on the TiO_2 surface. Therefore, Au nanoparticles act as capacitive junctions that improve the photoinduced current, leading to a spatial separation of charge carriers and therefore a decrease in the recombination rate in e^-−h^+ pairs, enhancing the catalyst stability.

CONCLUSIONS

In this work, we elucidate the effect that the Au NP decorated on TiO_2 has on the photogeneration, charge transfer, and trapping. By examining the effect of illumination on single Au NPs we were able to relate nanoscale observations with macroscopic results from TiO_2/AuNP−electrolyte interfaces under different conditions. By means of PA-KPFM, we have been able to achieve high-resolution SPV imaging of single Au NPs of 3 nm diameter simultaneously with the topographic image. This allowed us to compare the differential charge transfer to the Au NP and to the TiO_2 surface when the system was exposed to light of band gap energy and to measure its dependence on light irradiance.

Our results indicate that a substantial number of electrons are transferred from the TiO_2 to the metal nanoparticle, which increases with light intensity in a logarithmic fashion. The logarithmic increase was explained by the interplay between the bare TiO_2 surface space charge region and the metal−semiconductor space charge region and their dependence on irradiation intensity. Irradiation induces a reduction of the TiO_2 work function due to band flattening, which in turn produces a larger bending of the Schottky barrier at the interface between the titania TiO_2 surface and the metal nanoparticle, thus promoting electron transfer to the metal nanoparticle. Therefore, because of the fact that the reduction of the surface space charge region with light power has a logarithmic rate, a logarithmic behavior is also expected for the electron transfer versus irradiance, as our results indicate.

Finally, we have shown that the observed electrochemical behavior of TiO_2 photoelectrodes containing large amounts of Au NPs is in line with the conclusions obtained by PA-KPFM.

https://doi.org/10.1021/acsami.1c13662
ACS Appl. Mater. Interfaces 2021, 13, 50531−50538

This parallel study by PA-KPFM and electrochemical experiments provides a deeper understanding of the charge transfer to the metal NP and to the TiO_2 and allows us to correlate the photoinduced charge generation and transfer in Au/TiO_2 interfaces with the enhancement in photocatalytic H_2 production.

EXPERIMENTAL SECTION

TiO_2 Substrate Preparation. The TiO_2(110) surface (Nb doped by 0.05% of the total weight, Shinkosha, CO. LTD.) was annealed in a preheated furnace at 900 °C for 1 h under a continuous flow of air.

Au NP Fabrication and Deposition. The Au NPs were prepared by means of a magnetron-sputtering−multiple-ion-cluster source[33,34] and deposited on Nb-doped TiO_2(110) crystals that were previously annealed in air. This gas-phase synthesis produced crystalline Au NPs with a convex regular icosahedral structure.[35] Details of the sample preparation procedure are presented in the Supporting Information (section 4).

PA-KPFM Implementation and Calibration. A fiber-coupled LED (M365FP1, Thorlabs Inc.) was used for illuminating the sample (wavelength 365 nm). The light beam was introduced in the optical path of a Cypher ES (Asylum Research, Oxford Instruments) AFM head through a dichroic hot mirror. We checked the consistency and stability of the PtIr tip work function by performing AP-KPFM measurements on graphite because the CPD is insensitive to light exposure when the metal coating is intact. The illumination calibration was performed with the silicon photodiode (UV extended) S120VC from Thorlabs. More details can be found in the Supporting Information (section 13).

PA-KPFM Experiments. PA-KPFM was implemented by operating in noncontact amplitude modulation mode (AM-AFM) with phase-locked loop (PLL) detection and force gradient feedback.[36] In this technique, two different types of modulations were applied to the cantilever: (1) a mechanical excitation at its resonance frequency and (2) an electrical excitation at lower frequency. As the tip scanned the sample, three types of simultaneous feedback were performed: (1) topography feedback to keep the mechanical oscillation amplitude constant by regulating the tip−sample distance (AM-AFM);[37,38] (2) a phase-locked loop (PLL) nullifies the phase difference between the driving signal and the cantilever mechanical oscillation, keeping the oscillation at resonance by controlling the excitation frequency; (3) a bias voltage is applied to the tip in order to nullify the electrostatic force or force gradient.[39] Hence, the CPD between the tip and sample is obtained at each pixel, as described in published literature.[40,41] We used a Cypher ES (Asylum Research) AFM and ATEC-EFM (Nanosensors) cantilevers, with a resonance frequency of 85 kHz and a force constant of 2.8 N/m. For the applied electrical excitation, the chosen amplitude was 2 V (rms) at a frequency of 7 kHz.

A key point of our technique is to achieve stable noncontact operation. Topographic noncontact feedback relies on the attractive force between the tip and sample that decreases the oscillating amplitude of the cantilever as the tip approaches the surface, making possible noncontact imaging of the surface and simultaneous acquisition of topography, frequency, and CPD data in a single pass.[40−42] It should be noted that the resolution in the AFM images is determined by the diameter of the tip apex, which is around 40 nm in our experiments, as shown in the Supporting Information (Figure S5). Data processing was done using the free software WSxM (version 5.0).[43]

Photo(electro)chemical Experiments. The studies with single Au NPs on TiO_2 were complemented by spatially averaged studies (i.e., with many NPs on the TiO_2) using electro- and photoelectrochemical measurements in a three-electrode cell with a quartz window in an aqueous solution of 0.5 M Na_2SO_3 at pH 9. Both Au NPs/TiO_2 and bare TiO_2 samples (5 × 5 mm^2) were used as working electrodes. The counter electrode was a platinum wire, and a Ag/AgCl wire was used as the reference electrode. The currents, in the dark and under illumination and the voltage, were measured with a potentiostat−galvanostat PGSTAT302N equipped with an integrated impedance module FRAII. A modulation amplitude of 10 mV was used in the frequency range from 1 Hz to 10,000 Hz in the EIS measurements. The experiments were conducted under an argon flow of 50 sccm through the top of the cell. A UV LED lamp (80 mW/cm^2) was used as the light source. To measure the reaction products, the cell was connected to a gas chromatograph (Agilent micro-GC 490) equipped with a MS5A column at a temperature of 60 °C and a TDC detector.

ASSOCIATED CONTENT

Supporting Information

The Supporting Information is available free of charge at https://pubs.acs.org/doi/10.1021/acsami.1c13662.

> Kelvin Probe Force Microscopy (KPFM) operation principle; Surface Photovoltage (SPV) under illumination exposure in Kelvin Probe Force Microscopy; SPV decrease in the presence of a hole scavenger; Au NPs fabrication and deposition on the TiO_2(110) surface. Au NPs size analysis; TEM image of conductive tip apex; Length of the Schottky junction depleted region for finite and small Au nanoparticle; Theoretical calculation of the electrostatic interaction forces between tip and surface; Theoretical model for calculating electric charge inside the nanoparticle; Au NP on TiO_2 CPD image of large areas; Topography, VCPD and Resonance Frequency images of an Au NP on TiO_2(110) by means of KPFM; Evaluation of carbonaceous molecular species on TiO_2(110) by means of sum frequency generation spectroscopy; Photoelectrochemical characterization; AFM modification for light implementation and light calibration (PDF)

AUTHOR INFORMATION

Corresponding Authors

Monica Luna − *IMN-Instituto de Micro y Nanotecnología (CNM-CSIC), 28760 Tres Cantos, Spain;* orcid.org/0000-0002-7104-0726; Email: monica.luna@csic.es

Paul D. Ashby − *Molecular Foundry, Lawrence Berkeley National Laboratory, Berkeley, California 94720, United States;* orcid.org/0000-0003-4195-310X; Email: pdashby@lbl.gov

Miquel Salmeron − *Materials Sciences Division, Lawrence Berkeley National Laboratory, Berkeley, California 94720, United States; Materials Science and Engineering Department, University of California Berkeley, Berkeley, California 94720, United States;* orcid.org/0000-0002-2887-8128; Email: mbsalmeron@lbl.gov

Authors

Mariam Barawi − *Photoactivated Processes Unit, IMDEA-ENERGIA, 28935 Móstoles, Spain;* orcid.org/0000-0001-5719-9872

Sacha Gómez-Moñivas − *Departamento de Ingeniería Informática, Escuela Politécnica Superior, Universidad Autónoma de Madrid, 28049 Madrid, Spain;* orcid.org/0000-0003-2280-5021

Jaime Colchero − *Departamento de Física, Universidad de Murcia, 30100 Murcia, Spain*

Micaela Rodríguez-Peña − *IMN-Instituto de Micro y Nanotecnología (CNM-CSIC), 28760 Tres Cantos, Spain*

https://doi.org/10.1021/acsami.1c13662
ACS Appl. Mater. Interfaces 2021, 13, 50531−50538

Shanshan Yang − *Materials Sciences Division, Lawrence Berkeley National Laboratory, Berkeley, California 94720, United States;* orcid.org/0000-0003-1427-171X
Xiao Zhao − *Materials Sciences Division, Lawrence Berkeley National Laboratory, Berkeley, California 94720, United States;* orcid.org/0000-0003-1079-664X
Yi-Hsien Lu − *Molecular Foundry and Materials Sciences Division, Lawrence Berkeley National Laboratory, Berkeley, California 94720, United States;* orcid.org/0000-0001-6572-5553
Ravi Chintala − *Molecular Foundry, Lawrence Berkeley National Laboratory, Berkeley, California 94720, United States*
Patricia Reñones − *Photoactivated Processes Unit, IMDEA-ENERGIA, 28935 Móstoles, Spain*
Virginia Altoe − *Molecular Foundry, Lawrence Berkeley National Laboratory, Berkeley, California 94720, United States*
Lidia Martínez − *Instituto de Ciencia de Materiales de Madrid (ICMM-CSIC), 28049 Madrid, Spain;* orcid.org/0000-0002-9370-2962
Yves Huttel − *Instituto de Ciencia de Materiales de Madrid (ICMM-CSIC), 28049 Madrid, Spain;* orcid.org/0000-0002-3683-9890
Seiji Kawasaki − *Molecular Foundry and Materials Sciences Division, Lawrence Berkeley National Laboratory, Berkeley, California 94720, United States*
Alexander Weber-Bargioni − *Molecular Foundry, Lawrence Berkeley National Laboratory, Berkeley, California 94720, United States*
Victor A. de la Peña ÓShea − *Photoactivated Processes Unit, IMDEA-ENERGIA, 28935 Móstoles, Spain;* orcid.org/0000-0001-5762-4787
Peidong Yang − *Materials Sciences Division, Lawrence Berkeley National Laboratory, Berkeley, California 94720, United States; Department of Chemistry, University of California, Berkeley, California 94720, United States;* orcid.org/0000-0003-4799-1684

Complete contact information is available at: https://pubs.acs.org/10.1021/acsami.1c13662

Notes

The authors declare no competing financial interest.

■ ACKNOWLEDGMENTS

This work was supported by the Office of Basic Energy Sciences (BES) of the U.S. Department of Energy (DOE) under contract DE-AC02-05CH11231 through the Structure and Dynamics of Materials Interfaces Program (FWP KC31SM) and the Molecular Foundry. M.L. acknowledges funds from Comunidad de Madrid (P2018/EMT-4308), a Fulbright grant PRX16/00564, and the MCIU-AEI-FEDER-UE (RTI2018-096937-B-C22 and MAT2014-59772-C2-1-P). J.C. acknowledges financial support from Ministerio de Ciencia e Innovación (MICINN) and the European Union through the project PID2019-104272RB-C52. Also, Y.H. acknowledges financial support from MCIU through MAT2014-59772-C2-2-P and L.M. from EC through ERC-2013-SYG-610256. V.A.P.O. and M.B. acknowledge the financial support from EC through ERC CoG HyMAP 648319, MINECO PID2019-106315RB-I00 and ENE2017-89170-R, "Comunidad de Madrid" and European Structural Funds (FotoArt-CM project S2018/NMT-4367) and Fundación Ramón Areces (Art-Leaf project). M.B. also thanks the Juan de la Cierva Incorporación contract (IJC2019—042430-I). X.Z. was supported by the NSF-BSF 359 grant number 1906014. The authors thank Prof. Eran Edri, María Ujué González Sagardoy, and Judit Meseguer-Oliver for fruitful discussions and Asylum customer support for help with modifications of the AFM.

■ REFERENCES

(1) Schneider, J.; Matsuoka, M.; Takeuchi, M.; Zhang, J.; Horiuchi, Y.; Anpo, M.; Bahnemann, D. W. Understanding TiO_2 Photocatalysis: Mechanisms and Materials. *Chem. Rev.* **2014**, *114*, 9919−9986.
(2) Mamaghani, A. H.; Haghighat, F.; Lee, C.-S. Photocatalytic Oxidation Technology for Indoor Environment Air Purification: The State-of-the-Art. *Appl. Catal., B* **2017**, *203*, 247−269.
(3) Gupta, B.; Melvin, A. A.; Matthews, T.; Dash, S.; Tyagi, A. K. TiO_2 Modification by Gold (Au) for Photocatalytic Hydrogen (H_2) Production. *Renewable Sustainable Energy Rev.* **2016**, *58*, 1366−1375.
(4) Zhang, Z.; Yates, J. T. Band Bending in Semiconductors: Chemical and Physical Consequences at Surfaces and Interfaces. *Chem. Rev.* **2012**, *112*, 5520−5551.
(5) Collado, L.; Reynal, A.; Coronado, J. M.; Serrano, D. P.; Durrant, J. R.; de la Peña O'Shea, V. A. Effect of Au Surface Plasmon Nanoparticles on the Selective CO_2 Photoreduction to CH_4. *Appl. Catal., B* **2015**, *178*, 177−185.
(6) Collado, L.; Reynal, A.; Fresno, F.; Barawi, M.; Escudero, C.; Perez-Dieste, V.; Coronado, J. M.; Serrano, D. P.; Durrant, J. R.; de la Peña O'Shea, V. A. Unravelling the Effect of Charge Dynamics at the Plasmonic Metal/Semiconductor Interface for CO_2 Photoreduction. *Nat. Commun.* **2018**, *9*, 4986.
(7) Fontelles-Carceller, O.; Muñoz-Batista, M. J.; Conesa, J. C.; Fernández-García, M.; Kubacka, A. UV and Visible Hydrogen Photo-Production Using Pt Promoted Nb-doped TiO_2 Photo-Catalysts: Interpreting Quantum Efficiency. *Appl. Catal., B* **2017**, *216*, 133−145.
(8) Hernández Rodríguez, M. J.; Pulido Melián, E.; García Santiago, D.; González Díaz, O.; Navío, J. A.; Doña Rodríguez, J. M. NO Photooxidation with TiO_2 Photocatalysts Modified with gold and platinum. *Appl. Catal., B* **2017**, *205*, 148−157.
(9) Lin, S. D.; Bollinger, M.; Vannice, M. A. Low Temperature CO Oxidation over Au/TiO_2 and Au/SiO_2 Catalysts. *Catal. Lett.* **1993**, *17*, 245−262.
(10) Liu, Z. M.; Vannice, M. A. CO andO_2 Adsorption on Model Au-Ti02 Systems. *Catal. Lett.* **1997**, *43*, 51−54.
(11) Chen, C. J.; Osgood, R. M. Direct Observation of the Local-Field-Enhanced Surface Photochemical Reactions. *Phys. Rev. Lett.* **1983**, *50*, 1705−1708.
(12) Awazu, K.; Fujimaki, M.; Rockstuhl, C.; Tominaga, J.; Murakami, H.; Ohki, Y.; Yoshida, N.; Watanabe, T. A Plasmonic Photocatalyst Consisting of Silver Nanoparticles Embedded in Titanium Dioxide. *J. Am. Chem. Soc.* **2008**, *130*, 1676−1680.
(13) Di Vece, M.; Laursen, A. B.; Bech, L.; Maden, C. N.; Duchamp, M.; Mateiu, R. V.; Dahl, S.; Chorkendorff, I. Quenching of TiO_2 Photo Catalysis by Silver Nanoparticles. *J. Photochem. Photobiol., A* **2012**, *230*, 10−14.
(14) Ioannides, T.; Verykios, X. E. Charge Transfer in Metal Catalysts Supported on Doped TiO_2: A Theoretical Approach Based on Metal−Semiconductor Contact Theory. *J. Catal.* **1996**, *161*, 560−569.
(15) Fernandez-Torre, D.; Yurtsever, A.; Onoda, J.; Abe, M.; Morita, S.; Sugimoto, Y.; Pérez, R. Pt Atoms Adsorbed on $TiO_2(110)$-(1×1) Studied with Noncontact Atomic Force Microscopy and First-Principles Simulations. *Phys. Rev. B: Condens. Matter Mater. Phys.* **2015**, *91*, 075401.
(16) Matthey, D.; Wang, J. G.; Wendt, S.; Matthiesen, J.; Schaub, R.; Laegsgaard, E.; Hammer, B.; Besenbacher, F. Enhanced Bonding of Gold Nanoparticles on Oxidized $Ti0_2(110)$. *Science* **2007**, *315*, 1692−1696.

(17) Lira, E.; Hansen, J. Ø.; Merte, L. R.; Sprunger, P. T.; Li, Z.; Besenbacher, F.; Wendt, S. Growth of Ag and Au Nanoparticles on Reduced and Oxidized Rutile TiO_2(110) Surfaces. *Top. Catal.* **2013**, *56*, 1460−1476.
(18) Prauzner-Bechcicki, J. S.; Zajac, L.; Olszowski, P.; Jöhr, R.; Hinaut, A.; Glatzel, T.; Such, B.; Meyer, E.; Szymonski, M. Scanning Probe Microscopy Studies on the Adsorption of Selected Molecular Dyes on Titania. *Beilstein J. Nanotechnol.* **2016**, *7*, 1642−1653.
(19) Enevoldsen, G. H.; Glatzel, T.; Christensen, M. C.; Lauritsen, J. V.; Besenbacher, F. Atomic Scale Kelvin Probe Force Microscopy Studies of the Surface Potential Variations on the TiO2(110) Surface. *Phys. Rev. Lett.* **2008**, *100*, 236104.
(20) Sasahara, A.; Pang, C. L.; Onishi, H. Probe Microscope Observation of Platinum Atoms Deposited on the TiO2(110)-(1 x 1) Surface. *J. Phys. Chem. B* **2006**, *110*, 13453−13457.
(21) Hiehata, K.; Sasahara, A.; Onishi, H. Local Work Function Analysis of Pt/TiO_2 Photocatalyst by a Kelvin Probe Force Microscope. *Nanotechnology* **2007**, *18*, 084007.
(22) Stevanovic, A.; Ma, S.; Yates, J. T., Jr. Effect of Gold Nanoparticles on Photoexcited Charge Carriers in Powdered TiO_2−Long Range Quenching of Photoluminescence. *J. Phys. Chem. C* **2014**, *118*, 21275−21280.
(23) Lin, W.-H.; Wu, J.-J.; Chou, M. M. C.; Chang, Y.-M.; Yoshimura, M. Charge Transfer in Au Nanoparticle-Nonpolar ZnO Photocatalysts Illustrated by Surface-Potential-Derived Three-Dimensional Band Diagram. *J. Phys. Chem. C* **2014**, *118*, 19814−19821.
(24) Kokawa, R.; Ohta, M.; Sasahara, A.; Onishi, H. Kelvin Probe Force Microscopy Study of a Pt/TiO2 Catalyst Model Placed in an Atmospheric Pressure of N_2 Environment. *Chem.—Asian J.* **2012**, *7*, 1251−1255.
(25) Henning, A.; Günzburger, G.; Jöhr, R.; Rosenwaks, Y.; Bozic-Weber, B.; Housecroft, C. E.; Constable, E. C.; Meyer, E.; Glatzel, T. Kelvin Probe Force Microscopy of Nanocrystalline TiO2 Photoelectrodes. *Beilstein J. Nanotechnol.* **2013**, *4*, 418−428.
(26) Argondizzo, A.; Cui, X.; Wang, C.; Sun, H.; Shang, H.; Zhao, J.; Petek, H. Ultrafast multiphoton pump-probe photoemission excitation pathways in rutileTiO2(110). *Phys. Rev. B: Condens. Matter Mater. Phys.* **2015**, *91*, 155429.
(27) Zhang, Y.; Pluchery, O.; Caillard, L.; Lamic-Humblot, A.-F.; Casale, S.; Chabal, Y. J.; Salmeron, M. Sensing the Charge State of Single Gold Nanoparticles via Work Function Measurements. *Nano Lett.* **2015**, *15*, 51−55.
(28) Bednyi, B. l.; Baidus, N. V. Effect of Recombination in the Space Charge Region on the Illuminance Characteristics of the Surface Photo-emf of GaAs and lnP. *Semiconductors* **1993**, *27*, 620−622.
(29) Reshchikov, M. A.; Foussekis, M.; Baski, A. A. Surface Photovoltage in Undoped n-type GaN. *J. Appl. Phys.* **2010**, *107*, 113535.
(30) Kronik, L.; Shapira, Y. Surface Photovoltage Phenomena: Theory, Experiment, and Applications. *Surf. Sci. Rep.* **1999**, *37*, 1−206.
(31) Mora-Seró, I.; Villarreal, T. L.; Bisquert, J.; Pitarch, Á.; Gómez, R.; Salvador, P. Photoelectrochemical Behavior of Nanostructured TiO_2 Thin-Film Electrodes in Contact with Aqueous Electrolytes Containing Dissolved Pollutants: A Model for Distinguishing between Direct and Indirect Interfacial Hole Transfer from Photocurrent Measurements. *J. Phys. Chem. B* **2005**, *109*, 3371−3380.
(32) Clavero, C. Plasmon-Induced Hot-Electron Generation at Nanoparticle/Metal-Oxide Interfaces for Photovoltaic and Photocatalytic Devices. *Nat. Photonics* **2014**, *8*, 95−103.
(33) Llamosa, D.; Ruano, M.; Martínez, L.; Mayoral, A.; Roman, E.; García-Hernández, M.; Huttel, Y. The Ultimate Step Towards a Tailored Engineering of Core@Shell and Core@Shell@Shell Nanoparticles. *Nanoscale* **2014**, *6*, 13483−13486.
(34) Mayoral, A.; Llamosa, D.; Huttel, Y. A novel Co@Au structure formed in bimetallic core@shell nanoparticles. *Chem. Commun.* **2015**, *51*, 8442−8445.
(35) Martínez, L.; Mayoral, A.; Espiñeira, M.; Roman, E.; Palomares, F. J.; Huttel, Y. Core@shell, Au@TiO_x Nanoparticles by Gas Phase Synthesis. *Nanoscale* **2017**, *9*, 6463−6470.
(36) Colchero, J.; Gil, A.; Baró, A. M. Resolution Enhancement and Improved Data Interpretation in Electrostatic Force Microscopy. *Phys. Rev. B: Condens. Matter Mater. Phys.* **2001**, *64*, 245403.
(37) Luna, M.; Colchero, J.; Baró, A. M. Study of Water Droplets and Films on Graphite by Noncontact Scanning Force Microscopy. *J. Phys. Chem. B* **1999**, *103*, 9576−9581.
(38) de Pablo, P. J.; Colchero, J.; Luna, M.; Gómez-Herrero, J.; Baró, A. M. Tip-sample Interaction in Tapping-mode Scanning Force Microscopy. *Phys. Rev. B: Condens. Matter Mater. Phys.* **2000**, *61*, 14179.
(39) Gil, A.; Colchero, J.; Gómez-Herrero, J.; Baró, A. M. Electrostatic Force Gradient Signal: Resolution Enhancement in Electrostatic Force Microscopy and Improved Kelvin Probe Microscopy. *Nanotechnology* **2003**, *14*, 332−340.
(40) Minj, A.; Cros, A.; Garro, N.; Colchero, J.; Auzelle, T.; Daudin, B. Assessment of Polarity in GaN Self-Assembled Nanowires by Electrical Force Microscopy. *Nano Lett.* **2015**, *15*, 6770−6776.
(41) Manzano, C. V.; Caballero-Calero, O.; Hormeño, S.; Penedo, M.; Luna, M.; Martín-González, M. S. ZnO Morphology Control by Pulsed Electrodeposition. *J. Phys. Chem. C* **2013**, *117*, 1502−1508.
(42) Boisgard, R.; Michel, D.; Aimé, J. P. Hysteresis generated by attractive interaction: oscillating behavior of a vibrating tip-microlever system near a surface. *Surf. Sci.* **1998**, *401*, 199−205.
(43) Horcas, I.; Fernández, R.; Gómez-Rodríguez, J. M.; Colchero, J.; Gómez-Herrero, J.; Baro, A. M. WSXM: A Software for Scanning Probe Microscopy and a Tool for Nanotechnology. *Rev. Sci. Instrum.* **2007**, *78*, 013705.

https://doi.org/10.1021/acsami.1c13662
ACS Appl. Mater. Interfaces 2021, 13, 50531−50538